

Daniel Dutzler, Markus Seibald, Dominik Baumann, Frauke Philipp, Simon Peschke and Hubert Huppertz*

RbKLi₂[Li₃SiO₄]₄:Eu²⁺ an ultra narrow-band phosphor

<https://doi.org/10.1515/znb-2019-0102>

Received June 28, 2019; accepted July 4, 2019

Abstract: The new phosphor RbKLi₂[Li₃SiO₄]₄:Eu²⁺ was synthesized by different high-temperature solid-state reactions. It is accessible from the alkali metal carbonates, SiO₂, and Eu²⁺ as a luminous active cation either in closed tantalum ampoules or by conventional solid-state reaction in nickel crucibles, under a constant flow of forming gas. The structure of the thereby received rod-shaped crystals was solved and refined on the basis of single crystal X-ray diffraction data. The compound crystallizes isostructurally to CsKNa₂[Li₃SiO₄]₄ and forms a highly condensed network of LiO₄ and SiO₄ tetrahedra [*I*4/*m* (no. 87), *Z*=2, *a*=10.9508(6) and *c*=6.3334(3) Å]. It is a new member of the recently discovered family of alkali lithosilicate phosphors. Under excitation with UV to blue light, the compound exhibits interesting luminescence properties. Depending on the mode of synthesis, either green or blue luminescence of the samples is observed. Both emission profiles can be described as ultra-narrow-banded, since the full width at half maximum (fwhm) is below 0.2 eV. The green phosphor shows an emission maximum at 532 nm with a fwhm of 43.5 nm (0.193 eV) and the blue one at 474 nm with a fwhm of 24.8 nm (0.137 eV). Furthermore, the material presented here allows a more detailed localization of the luminescence center inside the structure, which may allow a better understanding of the luminescence properties of many other alkali lithosilicate phosphors.

Keywords: crystal structure; europium; high-temperature synthesis; lithosilicate phosphors; luminescence.

*Corresponding author: Hubert Huppertz, Institut für Allgemeine, Anorganische und Theoretische Chemie, Universität Innsbruck, Innrain 80–82, A-6020 Innsbruck, Austria, E-mail: hubert.huppertz@uibk.ac.at

Daniel Dutzler: Institut für Allgemeine, Anorganische und Theoretische Chemie, Universität Innsbruck, Innrain 80–82, A-6020 Innsbruck, Austria

Markus Seibald, Dominik Baumann, Frauke Philipp and Simon Peschke: OSRAM Opto Semiconductors GmbH, Mittelstetter Weg 2, D-86830 Schwabmünchen, Germany

1 Introduction

In modern technologies, phosphor-converted light-emitting diodes (pc-LEDs) are found nearly everywhere. Their usage is no longer limited to general indoor and outdoor lighting applications. To ensure a broad variety of illuminants, a significant number of novel phosphors has been discovered and developed in the last years. Additionally to the well-known alkaline earth (oxo)nitride phosphors, a number of new substance classes have proven to exhibit promising emission properties e.g. from the cyan up to the yellow spectral region. This includes alkali lithosilicates, nitridoberyllates, and oxonitridoberyllates. Typical examples from the substance class of alkali lithosilicates are the ultra-narrow blue emitting phosphor RbNa₃[Li₃SiO₄]₄:Eu²⁺ as well as the green emitters RbLi[Li₃SiO₄]₂:Eu²⁺ and NaK₇[Li₃SiO₄]₈:Eu²⁺ [1–6]. From the group of the recently discovered beryllate phosphors, the blue to cyan emitting compounds AELi₂[Be₄O₆]:Eu²⁺ (*A*E = Sr, Ba), Sr[Be₆ON₄]:Eu²⁺ [7, 8], and the yellow emitter SrBeO₂:Eu²⁺ have to be mentioned [9].

White LEDs also play an important role in today's display technologies. They are produced to enhance modern day liquid crystal displays (LCDs) and to achieve a larger color gamut and higher brightness with the advantage of a lower energy consumption [10–12]. Nowadays, two different technologies try to approach this problem. While multichip white LEDs, consisting of separately controlled blue, green, and red LED chips, exhibit an excellent color gamut, they face two major flaws. Firstly, the separate driving circuits for each LED are costly and secondly the green LED chip suffers from a poor efficiency, which leads to the so called “green gap” [10, 13]. Therefore, the use of pc-LEDs containing two phosphors (green and red) as backlighting units in liquid crystal monitors (LCD monitors) is preferred. Consequently, the reachable color gamut of such displays is limited by the color purity and color coordinates of the used phosphors [10].

Because of this, the development of narrow-band green- and red-emitting phosphors for use in the backlighting units of LCD displays was continuously driven forward in the last decade. The goal is to improve the color gamut in order to realize the most lifelike artificial display.

This can only be achieved by developing and combining phosphors with the desired peak positions, narrow emission bands, and high quantum efficiencies [14–16].

Commonly used pc-LEDs for backlighting are based on a blue emitting (In,Ga)N LED chip [17, 18], in combination with narrow-band red and narrow-band green phosphors. For modern devices, the current phosphors of choice are Y₃Al₅O₁₂:Ce³⁺ or β-SiAlON:Eu²⁺ [19–21], as the green component and (Sr,Ca)AlSiN:Eu²⁺ or K₂SiF₆:Mn⁴⁺ [22–24] as the red components. With regard to the red phosphor, Sr[LiAl₃N₄]:Eu²⁺ and the recently discovered ultra-narrow-band emitting compound SrLi₂Al₂O₂N₂:Eu²⁺ [25, 26] could be promising candidates for future applications.

Presently, the display color gamut is mainly limited by the color coordinates of the green phosphor. Due to the fact, that the human eye is most sensitive in the green spectral region, the main challenge is to improve the green phosphors to reach a better positioning inside the CIE diagram. State of the art green emitters involve quantum dots (QDs) and rare earth doped phosphors, such as the previously mentioned β-SiAlON:Eu²⁺, the ortho-silicate (Ba,Sr)₂SiO₄:Eu²⁺, and the oxonitridosilicate SrSi₂O₂N₂:Eu²⁺ [27–29].

In this contribution, we report on the synthesis and characterization of a new alkali lithosilicate phosphor with the composition RbKLi₂[Li₃SiO₄]₄:Eu²⁺ (RKLSO:Eu²⁺). First samples showed an ultra-narrow-banded emission in the green spectral region, making it an interesting phosphor for a potential usage in pc-LEDs for backlighting units. Further research revealed that RKLSO:Eu²⁺ can also emit in the blue spectral region. The origin of both emission bands is investigated based on structure-property relationships.

2 Experimental section

2.1 Synthesis

The compound RbKLi₂[Li₃SiO₄]₄:Eu²⁺ was first synthesized by firing a mixture of Rb₂CO₃ (57.90 mg, 0.251 mmol, ChemPur, 99.9%), K₂CO₃ (11.55 mg, 0.084 mmol, ChemPur, 99.9%), SiO₂ (20.09 mg, 0.334 mmol, Fluka, >99.9%), and Li metal (9.28 mg, 1.337 mmol, Sigma Aldrich, 99%) in the molar ratio of 3:1:4:16. The starting materials were thoroughly ground in an agate mortar, filled into a Ta ampoule, and sealed via arc-welding. All preparation steps were carried out under inert gas atmosphere (Ar 5.0, Messer Austria GmbH). The ampoules were placed into evacuated silica-glass tubes, heated to 800–850°C within 4 h, maintained at that temperature for 48 h, and subsequently

cooled to 400°C over a period of 40 h. Eu₂O₃ was used as the source for Eu²⁺ as a luminous active cation.

The product was an inhomogeneous mixture of a highly air sensitive phase with metallic luster, and green, rod-shaped crystals, which were identified as the title compound.

When the composition of the green compound RbKLi₂[Li₃SiO₄]₄:Eu²⁺ had been clarified, bulk samples could be synthesized in an open system from the stoichiometric mixture of Rb₂CO₃ (39.15 mg, 0.170 mmol, ChemPur, 99.9%), K₂CO₃ (21.30 mg, 0.154 mmol, ChemPur, 99.9%), SiO₂ (74.08 mg, 1.233 mmol, Fluka, >99.9%), Li₂O (64.38 mg, 2.155 mmol, Alfa Aesar, 99.5%), and 1 mol-% Eu₂O₃ (1.08 mg, 0.003 mmol, Treibacher, >99.9%). The starting materials were weighed and thoroughly ground in an agate mortar at ambient conditions and filled into a Ni crucible. The open crucible was placed in a tube furnace and sintered at 450°C for 24 h, before firing it at 750°C for another 8 h under a constant flow of forming gas (H10, Messer GmbH). Due to the moisture sensitivity of some of the starting materials, all manipulations were carried out using an inert gas filled glovebox (MBraun, O₂ < 1 ppm, H₂O < 1 ppm).

Depending on the synthetic conditions, either green or blue emitting crystals of the same phase could be obtained. While the synthesis in ampoules always resulted in green luminescent crystals, a synthesis in the open system yielded a mixture of both the green and the blue emitting forms.

2.2 Single crystal X-ray diffraction

The crystal structure of green luminescent RbKLi₂[Li₃SiO₄]₄:Eu²⁺ was solved and refined on the basis of single crystal X-ray diffraction data, obtained from a Bruker D8 Quest diffractometer (MoKα radiation, λ = 0.7107 Å). The programs SAINT [30] and SADABS [31] were applied for data processing and a multi-scan absorption correction. The structure was solved in WINGX [32] using Direct Methods provided by SHELXS. The structural refinement was carried out by the method of least-squares using SHELXL [33].

Additionally, single crystals of the blue luminescent RbKLi₂[Li₃SiO₄]₄:Eu²⁺ phase were also characterized based on data from a Bruker D8 Quest diffractometer with CuKα radiation (λ = 1.5418 Å).

Further details on the crystal structure investigation on a green and a blue luminescent single crystal of RbKLi₂[Li₃SiO₄]₄:Eu²⁺ can be obtained from The Cambridge Crystallographic Data Centre via www.ccdc.cam.ac.uk/data_request/cif under the depository numbers CCDC 1922237 (green) and CCDC 1936593 (blue).

2.3 Powder X-ray diffraction

Powder X-ray diffraction data was collected on a STOE STADI P diffractometer ($\text{MoK}\alpha_1$ radiation, $\lambda = 0.7093$ nm) with a Ge(111) monochromator and a Mythen 1K detector in Debye-Scherrer geometry. The Rietveld refinement was performed using TOPAS 4.2 [34].

2.4 Luminescence

The emission spectra of green luminescent $\text{RbKLi}_2[\text{Li}_3\text{SiO}_4]_4:\text{Eu}^{2+}$ single crystals were recorded using a setup equipped with a blue laser diode ($\lambda = 448$ nm, THORLABS, Newton, NJ, USA) and a CCD Detector (AVA AvaSpec 2048, AVANTES, Apeldoorn, Netherlands). Prior to the experiments, a tungsten-halogen calibration lamp was used for a spectral radiance calibration of the setup. The software AVA AVASOFT version 7 was used for data handling.

Spectroscopic data of blue luminescent $\text{RKLSo}:\text{Eu}^{2+}$ single crystals, mounted on glass fibers, was recorded using a setup equipped with a UV to blue laser diode ($\lambda = 408$ nm, Thorlabs), single-mode optical fibers S405XP (Thorlabs), and a QE 65000 spectrometer (Ocean Optics).

In order to determine the luminescence properties of powder samples, a Fluoromax 4 spectrophotometer (Horiba) was used. The emission spectrum was measured in the wavelength range between 410 and 750 nm (step size 1 nm) using an excitation wavelength of 400 nm. Excitation spectra, monitored at the corresponding maximum intensity, and temperature dependent spectra were measured using the same method.

2.5 EDX spectroscopy and electron microscopy

In order to study the morphology and to analyze the chemical composition of the synthesized crystals, a SUPRATM35 scanning electron microscope (SEM, Carl Zeiss, field emission) equipped with a Si/Li EDX detector (Oxford Industries, model 7426) was used.

3 Results and discussion

Syntheses according to the above mentioned routes yielded single crystals and powder samples of the novel phosphor $\text{RbKLi}_2[\text{Li}_3\text{SiO}_4]_4:\text{Eu}^{2+}$. However, single crystals of

this material showed two different emission peaks, either in the blue or the green spectral region, upon excitation with near-UV to blue light. To prove that both variants have the same basic crystal structure, they were sorted with respect to their luminescence and analyzed separately via single crystal X-ray diffraction. The results are presented in the following. Furthermore, EDX measurements were performed on both sorts of crystals revealing an identical Rb:K:Si ratio of 1:1:4 in both cases, confirming the nominal composition of the materials as $\text{RbKLi}_2[\text{Li}_3\text{SiO}_4]_4:\text{Eu}^{2+}$.

3.1 Crystal structure

The crystal structure of the compound was first investigated by single crystal X-ray diffraction on the green luminescent phase. The structure of $\text{RbKLi}_2[\text{Li}_3\text{SiO}_4]_4:\text{Eu}^{2+}$ ($\text{RKLSo}:\text{Eu}^{2+}$) was solved and refined in the tetragonal space group $I4/m$. Details on the crystal structure solution and the refinement are given in the Tables 1 and 2. Atomic coordinates, displacement parameters, and a list of the interatomic distances and selected angles are shown in the Tables 3–5.

$\text{RKLSo}:\text{Eu}^{2+}$ crystallizes in the tetragonal space group $I4/m$ (no. 87) with the cell parameters $a = 10.9508(6)$ and $c = 6.3334(3)$ Å. The compound is isostructural to the phases $\text{RbNa}_3[\text{Li}_3\text{SiO}_4]_4$ (RNLSO), $\text{CsNa}_2\text{K}[\text{Li}_3\text{SiO}_4]_4$ (CNKLSO), already discovered by Hoppe, and the recently reported $\text{RbNa}_2\text{K}[\text{Li}_3\text{SiO}_4]_4$ (RNKLSO) [3, 35, 36].

The crystal structure of $\text{RKLSo}:\text{Eu}^{2+}$ consists of a three-dimensional, highly condensed network of corner- and edge-sharing LiO_4 and SiO_4 tetrahedra (Fig. 1), where the SiO_4 tetrahedra are isolated from each other and connect only with LiO_4 tetrahedra. These tetrahedra form endless *vierer* ring [37] channels along [001].

Two characteristic channels can be differentiated (Figs. 1 and 2), in the following named CH1 and CH2, which are interconnected via common edges forming a third channel. The cavities in this third channel are too small to host any metal cations.

CH1 incorporates the heavy alkali cations potassium and rubidium on two crystallographically distinguishable sites (Rb1 and K2, Fig. 2, left). These two sites are arranged alternately in the form of endless strings along [001]. Both sites show a highly symmetric eight-fold cuboid coordination [$\text{K}-\text{O} = 2.809(1)$ Å $8\times$ and $\text{Rb}-\text{O} = 3.042(1)$ Å $8\times$]. The K2 site is solely occupied by potassium, while the Rb1 site shows a partial substitution of rubidium by potassium (≈ 6 –14%). The relatively large ionic radii of K^+ and especially Rb^+ lead to a strong distortion of the

Table 1: Crystal data and structure refinement of green luminescent RbKLi₂[Li₃SiO₄]₄:Eu²⁺ for both proposed models (standard deviations in parentheses).

Empirical formula	RbKLi ₂ [Li ₃ SiO ₄] ₄		RbKLi ₂ [Li ₃ SiO ₄] ₄ :Eu ²⁺
Crystal system		Tetragonal	
Space group		<i>I</i> 4/ <i>m</i>	
Single crystal data			
Radiation/wavelength λ , Å		MoK α /0.71073	
<i>a</i> , Å		10.9508(6)	
<i>c</i> , Å		6.3334(3)	
Cell volume, Å ³		759.50(9)	
Formula units per unit cell		2	
ρ_{calcd} , g cm ⁻³		2.63	
μ , mm ⁻¹		3.9	
<i>T</i> , K		173(2)	
<i>F</i> (000), <i>e</i>		564	
Profile range, deg		2.6 ≤ θ ≤ 29.4	
Index ranges, <i>hkl</i>		±19; ±19; ±11	
Total reflections		18 754	
Independent reflections/ <i>R</i> _{int}		1213/0.0361	
Refined parameters		53	
Absorption correction		Multiscan (SADABS)	
Goodness-of-fit on <i>F</i> ²	1.099		1.107
Final indices <i>R</i> ₁ / <i>wR</i> ₂ (all data)	0.0284/0.0751		0.0279/0.0743
Largest diff. peak/hole, e Å ⁻³	+1.17/−1.44		+0.33/−1.39
Errors	Li3 and Li4 NPD		None

Table 2: Crystal data and structure refinement of blue luminescent RbKLi₂[Li₃SiO₄]₄:Eu²⁺ single crystals and the data received by the Rietveld refinement on the bulk powder sample (standard deviations in parentheses).

Empirical formula	RbKLi ₂ [Li ₃ SiO ₄] ₄ :Eu ²⁺		
Crystal system	Tetragonal		
Space group	<i>I</i> 4/ <i>m</i>		
Single crystal data			
Radiation/wavelength λ , Å		CuK α /1.54178	
<i>a</i> , Å	10.9682(2)	10.960(1)	10.977(2)
<i>c</i> , Å	6.3403(1)	6.3458(6)	6.3457(9)
Cell volume, Å ³	762.75(9)	762.3(2)	764.6(2)
Formula units per unit cell		2	
ρ_{calcd} , g cm ⁻³	2.57	2.57	2.563
μ , mm ⁻¹	10.8	10.8	10.7
<i>T</i> , K		296(2)	
<i>F</i> (000), <i>e</i>		564	
Profile range, deg		5.7 ≤ θ ≤ 67.9	
Index ranges, <i>hkl</i>		−12 ≤ <i>h</i> ≤ 11; −12 ≤ <i>k</i> ≤ 13; −7 ≤ <i>l</i> ≤ 7	
Total reflections	2716	2518	3481
Independent reflections/ <i>R</i> _{int}	382/0.028	376/0.0258	379/0.0359
Refined parameters		53	
Absorption correction		Multiscan (SADABS)	
Goodness-of-fit on <i>F</i> ²	1.184	1.148	1.121
Final <i>R</i> ₁ / <i>wR</i> ₂ indices (all data)	0.020/0.0471	0.0223/0.0556	0.0181/0.0454
Largest diff. peak/hole, e Å ⁻³	+0.44/−0.31	+0.31/−0.41	+0.44/−0.31
Powder data			
Radiation/wavelength λ , Å		MoK α ₁ /0.7093	
<i>a</i> , Å		10.9706(2)	
<i>c</i> , Å		6.3412(2)	
Cell volume, Å ³		763.19(4)	
2 θ range, deg		2.1–42.0	
<i>R</i> _{exp} , %		3.55	
<i>R</i> _{wp} , %		3.46	
<i>R</i> _p , %		2.73	

Table 3: Atomic coordinates and displacement parameters of RKLSo:Eu^{2+} for the structural model with the Li4 site occupied by Li^+ (top) and for the refinement model with Eu^{2+} (bottom).

Atom	Wyckoff	x	y	z	U_{eq}	SOF
Rb1/K1	2a	1/2	1/2	1/2	0.01042(8)	0.92/0.08
K2	2b	1/2	1/2	0	0.00337(9)	1
Si1	8h	0.21698(3)	0.42223(3)	0	0.00275(8)	1
Li1	16i	0.2556(3)	0.6125(3)	0.2439(4)	0.0114(4)	1
Li2	8h	0.0762(3)	0.7134(3)	0	0.0098(5)	1
Li3	4c	0	1/2	0	0.005(1)	1/3
Li4	4d	0	1/2	3/4	-0.0169(7)	2/3
O1	8h	0.09757(9)	0.33296(9)	0	0.0050(2)	1
O2	16i	0.29721(6)	0.40485(7)	0.2160(2)	0.0056(2)	1
O3	8h	0.16438(9)	0.56279(9)	0	0.0046(2)	1
Rb1/K1	2a	1/2	1/2	1/2	0.01043(7)	0.92/0.08
K2	2b	1/2	1/2	0	0.00334(8)	1
Si1	8h	0.21697(3)	0.42224(3)	0	0.00275(7)	1
Li1	16i	0.2558(3)	0.6121(3)	0.2439(4)	0.0114(4)	1
Li2	8h	0.0761(3)	0.7134(3)	0	0.0097(5)	1
Li3	4c	0	1/2	0	0.017(1)	0.98
Eu1	4d	0	1/2	3/4	0.003(2)	0.02
O1	8h	0.09756(8)	0.33295(8)	0	0.0050(2)	1
O2	16i	0.29724(6)	0.40488(6)	0.2160(2)	0.0056(2)	1
O3	8h	0.16440(9)	0.56278(8)	0	0.0046(2)	1

Table 4: Interatomic distances (Å) and mean bond lengths in RKLSo (standard deviations in parentheses) for both structural models.

Rb1/K1–O2	3.0419(8) 8×	K2–O2	2.8086(8) 8×	Li3–O3	1.927(1) 2×	Li4–O3	2.4938(8) 4×
				–O1	2.118(1) 2×	–O1	2.6448(8) 4×
\emptyset	3.042	\emptyset	2.809	\emptyset	2.023	\emptyset	2.569
Si1–O1	1.633(1)	Li1–O1	1.897(3)	Li2–O3	1.897(3)		
–O2	1.6369(8) 2×	–O3	1.918(3)	–O1	1.918(3)		
–O3	1.643(1)	–O2	1.919(3)	–O2	2.030(2) 2×		
		–O2	2.326(3)				
\emptyset	1.638	\emptyset	2.015	\emptyset	1.969		
Rb1/K1–O2	3.0419(8) 8×	K2–O2	2.8086(8) 8×	Li3–O3	1.927(1) 2×	Eu1–O3	2.4941(7) 4×
				–O1	2.116(1) 2×	–O1	2.6448(8) 4×
\emptyset	3.042	\emptyset	2.809	\emptyset	2.022	\emptyset	2.570
Si1–O1	1.633(1)	Li1–O1	1.897(3)	Li2–O3	1.911(3)		
–O2	1.6369(8) 2×	–O3	1.918(3)	–O1	1.969(3)		
–O3	1.643(1)	–O2	1.919(3)	–O2	2.030(2) 2×		
		–O2	2.321(3)				
\emptyset	1.638	\emptyset	2.014	\emptyset	1.985		

With either Li^+ (top) or Eu^{2+} located at the Li4 site (bottom).

surrounding LiO_4 tetrahedra with Li–O distances of 1.897(3)–2.326(3) Å. This distorted tetrahedron exhibits one rather long Li–O bond between Li1 and O2 with a length of 2.326(3) Å. Therefore, the surrounding of Li1 is better described as a 3+1 coordination in the form of an elongated trigonal pyramid. Furthermore, MAPLE calculations confirm a lower contribution of only 0.125 of the Li1–O2 bond towards the effective coordination number of lithium. Compared to the usual ECoN values in the range of 0.8–1.0 for Li–O bonds in a tetrahedral coordination of

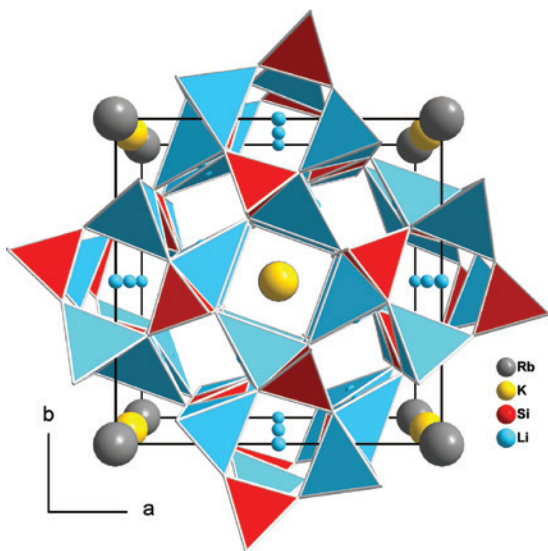
lithium, the value obtained for the title compound is significantly lower.

CH2 (Fig. 2, right) consists of *vierer* rings built up from two LiO_4 (blue) and two SiO_4 tetrahedra (red). According to the results for the first green emitting single crystal analyzed, this channel hosts two possible atom sites for Li, in the following named Li3 and Li4 (Fig. 2, right). Variations of the occupancies inside CH2 allow the refinement of two different structure models. Both are discussed in the following.

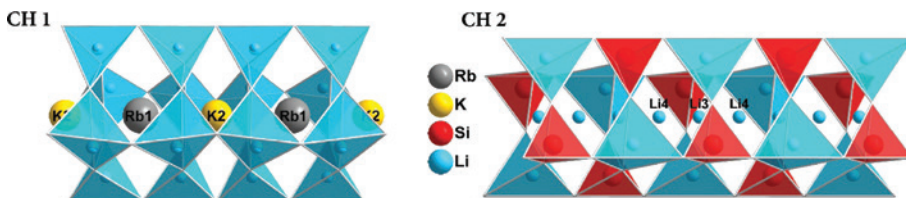
Table 5: Anisotropic displacement parameters U_{ij} (Å²) of RKLSo (standard deviations in parentheses) for both structural models.

Atom	U_{11}	U_{22}	U_{33}	U_{23}	U_{13}	U_{12}
Rb1/K1	0.01197(9)	0.01197(9)	0.0073(2)	0	0	0
K2	0.0031(1)	0.0031(1)	0.0040(2)	0	0	0
Si1	0.0027(2)	0.0027(2)	0.0029(2)	0	0	0.00020(9)
Li1	0.0097(9)	0.018(1)	0.0070(9)	-0.0010(7)	0.0009(6)	-0.0047(7)
Li2	0.008(1)	0.009(1)	0.012(2)	0	0	0.0015(9)
Li3	-0.003(2)	-0.001(2)	0.018(3)	0	0	0.001(2)
Li4	-0.0185(9)	-0.0185(9)	-0.014(2)	0	0	0
O1	0.0047(4)	0.0054(4)	0.0051(4)	0	0	-0.0018(3)
O2	0.0055(3)	0.0077(3)	0.0036(3)	0.002(2)	-0.0008(2)	0.0018(2)
O3	0.0052(4)	0.0031(4)	0.0054(4)	0	0	0.0010(3)
Rb1/K1	0.01199(8)	0.01199(8)	0.0073(2)	0	0	0
K2	0.0031(1)	0.0031(1)	0.0039(2)	0	0	0
Si1	0.0027(2)	0.0027(2)	0.0029(2)	0	0	0.00020(8)
Li1	0.0101(8)	0.0174(9)	0.0067(8)	-0.0011(7)	0.0009(6)	-0.0050(7)
Li2	0.008(1)	0.009(1)	0.012(2)	0	0	0.0016(8)
Li3	0.008(2)	0.011(2)	0.031(3)	0	0	0.001(2)
Eu1	0.002(2)	0.002(2)	0.006(2)	0	0	0
O1	0.0046(4)	0.0054(4)	0.0051(4)	0	0	-0.0018(3)
O2	0.0056(3)	0.0076(3)	0.0036(3)	0.002(2)	-0.0008(2)	0.0018(2)
O3	0.0052(3)	0.0032(3)	0.0054(3)	0	0	0.0009(3)

With either Li⁺ (top) or Eu²⁺ located at the Li4 site (bottom).

**Fig. 1:** Structure model of RKLSo with fully occupied Li3 sites viewed along $[00\bar{1}]$.

The first refinement was carried out with the assumption that both possible atom sites are occupied with lithium. The Li3 site shows a square-planar coordination with Li–O distances of 1.927(1)–2.116(1) Å (Fig. 3). Additionally, some residual electron density (Table 6) was found in CH2 at the position $(0\ 1/2\ 3/4)$. This electron density has been interpreted as a second possible atom site for lithium, the Li4 site. Figure 3 clearly shows that the cation Li4 is located in the center of four SiO₄ and four LiO₄ tetrahedra possessing an eight-fold cuboid coordination by oxygen atoms. At this site, the Li–O bond lengths range between 2.494(1) and 2.649(1) Å. According to the literature, the average Li–O bond length in an eight-fold coordination is given as 2.28 Å, so an occupation with lithium is unlikely [38]. Furthermore, to maintain electro-neutrality both sites cannot be fully occupied. Additionally, the short distance of 1.583(1) Å between the positions of Li3 and Li4 reveals that a simultaneous occupation of

**Fig. 2:** Detailed view of the two different occupied channels forming the structure of RKLSo. The left part shows a sidelong view of CH1 containing the heavy alkali cations with an alternating sequence of rubidium (Rb1) and potassium (K2) cations. The right part shows CH2 with the lighter alkali cation lithium occupying both possible sites (Li3 and Li4).

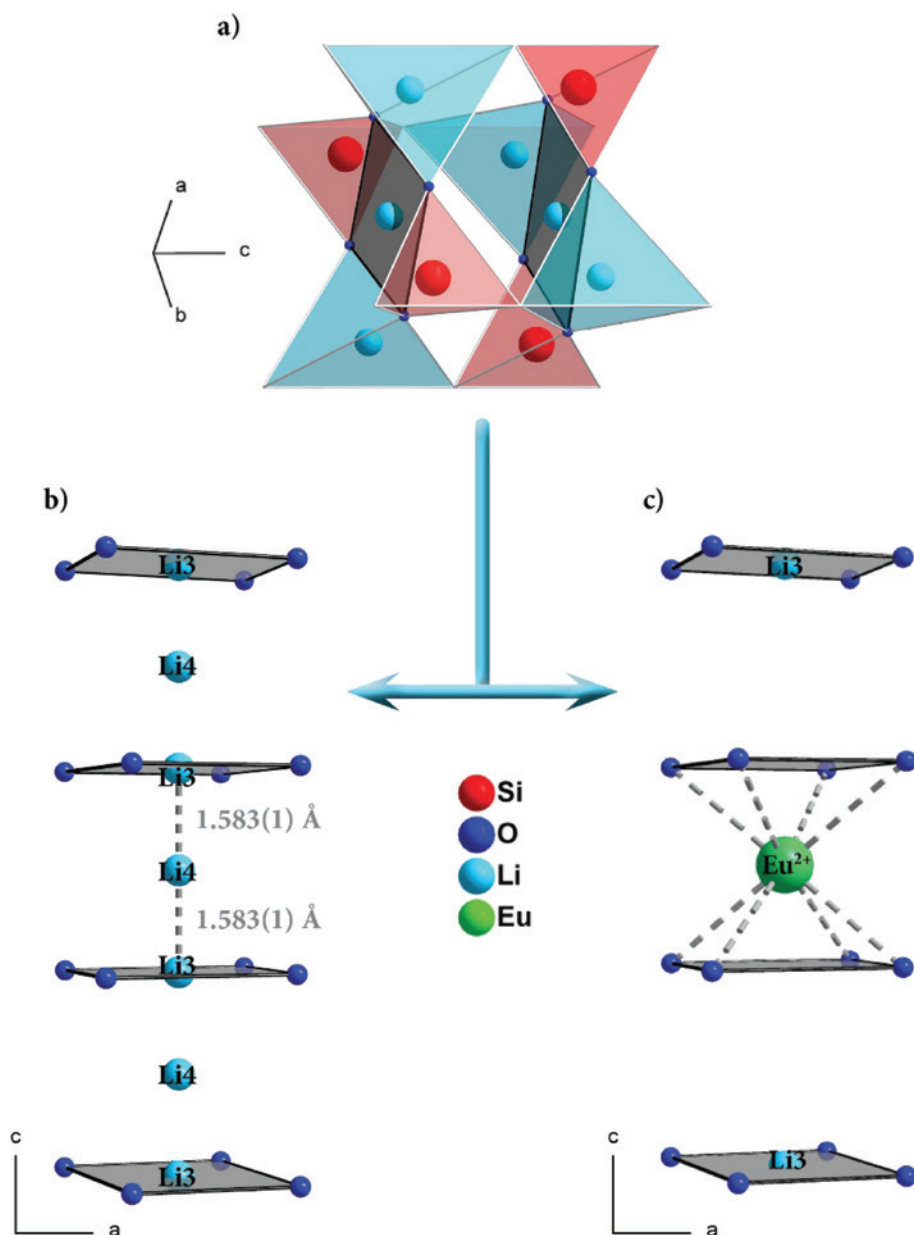


Fig. 3: Section of the structure of RKLSo with a) showing a detailed view of the lithium containing channel CH2 with Li3 in the square planar coordination. Part b) shows the positioning of the lithium cations Li3 and Li4 according to the first structure models proposed by Hoppe, while c) shows the configuration according to the second structural model with Eu^{2+} positioned at the Li4 site.

Table 6: Residual electron density at $(0, 1/2, 3/4)$ for the three measured blue emitting single crystals, compared to the first discovered green emitting single crystal, when the “Li4” site is left unoccupied.

Single crystal	Wyckoff	x, y, z	$e \text{ \AA}^{-3}$	R_1	wR_2	GoF
Green	4d	0, 1/2, 3/4	8.68	0.0424	0.1135	1.105
Blue1	4d	0, 1/2, 3/4	0.00	0.0200	0.0471	1.184
Blue2	4d	0, 1/2, 3/4	0.13	0.0223	0.0550	1.148
Blue3	4d	0, 1/2, 3/4	0.12	0.0181	0.0454	1.121

both neighboring positions is not possible (Fig. 3b). This exclusion was also observed in the single crystal refinement, which resulted in a $2/3^{\text{rd}}$ and a $1/3^{\text{rd}}$ occupancy of the Li3 and Li4 site, respectively.

Such a configuration was once reported by Hoppe for his “stuffed pyrgoms”, more specifically for the compound $\text{CsKNaLi}[\text{Li}_3\text{SiO}_4]_4$ [35]. This structure likewise consists of two distinguishable channels, one for the heavy alkali cations cesium and potassium and one for the lighter cations sodium and lithium. In $\text{CsKNaLi}[\text{Li}_3\text{SiO}_4]_4$,

Na and Li are arranged in the same way as the cations Li3 and Li4 in RbKLi₂[Li₃SiO₄]₄:Eu²⁺ resulting in a close proximity of the two sites with a distance of 1.6 Å. The Na and Li sites are only half occupied. Hoppe suggested different models to give a reasonable explanation for these findings. One structure model is based on the formation of domains, where the Na/Li channel is occupied solely by sodium cations in one part of the domains and exclusively by lithium cations in the other part. A different structure model could be an alternating stacking of the cations in the channels [35]. In the case of RKLSo:Eu²⁺ presented here, this would result in channels primarily hosting lithium cations at the Li3 or the Li4 site, always ensuring that a square-planar coordinated Li⁺ cation and a cuboid coordinated Li⁺ will never be adjacent to each other. These structural models would mean that RbKLi₂[Li₃SiO₄]₄:Eu²⁺ is isotypic to CsKNaLi[Li₃SiO₄]₄. However, the structure refinement of RbKLi₂[Li₃SiO₄]₄:Eu²⁺ based on these models of Hoppe always yielded non-positive definite atoms for the Li3 and Li4 site.

Therefore, an additional structural model for RbKLi₂[Li₃SiO₄]₄:Eu²⁺ is proposed, which includes the activator cation Eu²⁺ in the refinement. In this model, some of the previously designated atom sites Li4 in CH2 are now occupied by europium. These Eu²⁺ cations are eight-fold coordinated by oxygen anions in a cuboid manner (Fig. 3c). With Eu–O distances of 2.4941(7) Å (4 ×) and 2.6448(8) Å (4 ×) leading to a mean value of 2.57 Å, the coordination corresponds to the mean expected bond length between Eu²⁺ and O²⁻ given in the literature (2.61 Å) [38]. The crystallographic site Li4 would thus be more suitable to host europium cations than lithium cations.

The crystal structure refinement with this hypothesis resulted in a model where the Li3 site is almost fully occupied, while the previously as Li4 site described position is now occupied by ≈1.8% Eu²⁺. This value correlates well to the formal content of the activator according to the initial weight. The proposed Eu site is highly symmetric and surrounded by four LiO₄ and four SiO₄ tetrahedra. The structure refinement resulted in slightly better *R* values and most importantly, the residual electron density was slightly lower, compared to a site occupation with Li⁺ cations.

The plausibility of this structural model for the green luminescent phase, where lithium is only located at the Li3 site, was later also proven on single crystal data of the blue luminescent phase. Even though these crystals showed a blue luminescence upon excitation and therefore, clearly contain Eu²⁺ as an activator, no residual electron density could be found in three measured single crystals at the atom site previously named the Li4 site

(Table 6). Additionally, a Rietveld refinement of the blue luminescent powder was performed. The refinement is in good agreement with the single crystal refinement of the blue phase ($a=10.9706(2)$, $c=6.3412(2)$ Å) (Fig. 4), further proving the plausibility of the structural model with the Li4 site unoccupied.

For the green luminescent phase, a clear mechanism for charge compensation can be postulated. If Eu²⁺ is located on the Li4 site, both neighboring Li⁺ cations positions must be unoccupied (Fig. 3c). A simultaneous occupation of both positions would lead to absurdly short distances of 1.54 Å between Eu²⁺ and Li⁺. To guarantee electro-neutrality, one Eu²⁺ cation always substitutes two Li⁺ cations.

When comparing the structural models proposed here for RKLSo:Eu²⁺ to that of the above mentioned isostructural compounds RNLSo and C/RNKLSo, the great similarities are obvious. However, the structure reported here is the first one to host a channel incorporating only lithium cations in the square planar coordination, while the other three compounds have sodium cations located at the cuboid coordinated atom site.

3.2 Lattice energy calculations

To prove the electrostatic consistency of the crystal structure and the two proposed models, MAPLE calculations (Madelung Part of Lattice Energy) of the lattice energy were carried out (Table 7). The calculated partial MAPLE values for the ions Rb⁺, K⁺, Li⁺, Si⁴⁺, and O²⁻ are in good accordance with reference values [2, 35]. Furthermore, the MAPLE value for RbKLi₂[Li₃SiO₄]₄ was calculated to 87748.0 kJ mol⁻¹ and compared to the stoichiometric sum of the compounds Rb₂O, K₂O, Li₂O, and SiO₂ (88114.2 kJ mol⁻¹).

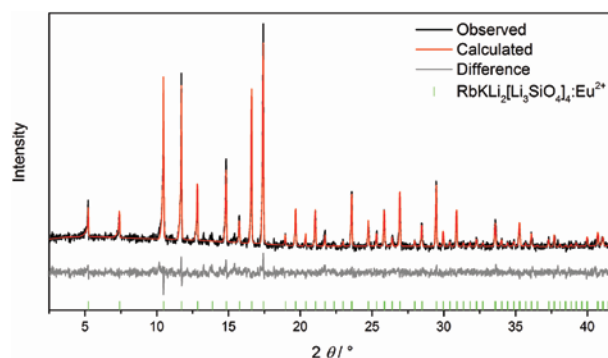


Fig. 4: Rietveld fit of blue luminescent RbKLi₂[Li₃SiO₄]₄:Eu²⁺ based on PXRD data (MoK α_1 , $\lambda=0.7093$ Å). The refinement is based on the structural model, where only the Li3 site is occupied.

Table 7: Partial MAPLE values for RKLSo (in kJ mol^{-1}) and a comparison of the MAPLE values to the oxides Rb_2O , K_2O , Li_2O , and SiO_2 .

Atom	Rb1/K1	K2	Si1	O1	O2	O3	Li1	Li2	Li3
Partial MAPLE values	486.4	422.9	8953.7	2621.5	2512.2	2681.7	691.5	759.3	572.1
Calcd. MAPLE for $\text{RbKLi}_2[\text{Li}_3\text{SiO}_4]_4$ (Li3 occupied, Li4 vacant) in kJ mol^{-1}									87748.0
Calcd. MAPLE for the educt compounds in kJ mol^{-1}									88114.2
Deviation in %									0.4
Atom	Rb1/K1	K2	Si1	O1	O2	O3	Li1	Li2	Li4
Partial MAPLE values	486.5	422.9	8979.4	2590.3	2514.0	2634.0	689.5	766.4	478.7
Calcd. MAPLE for $\text{RbKLi}_2[\text{Li}_3\text{SiO}_4]_4$ (Li3 vacant, Li4 occupied) in kJ mol^{-1}									87374.5
Calcd. MAPLE for the educt compounds in kJ mol^{-1}									88114.2
Deviation in %									0.8

Calculations were performed on the two calculated modifications of RKLSo, where either the Li3 site (top) or the Li4 site is fully occupied (bottom).

The result is only a slight deviation of 0.4% for the structural model, when presumed that only the Li3 site is occupied. For comparison, the calculation of a structural model where only the Li4 site is occupied, results in a substantially larger deviation (0.8%) and especially the partial MAPLE value for Li4 with $478.7 \text{ kJ mol}^{-1}$ is too low compared to 611 kJ mol^{-1} for lithium in Li_2O . Therefore, the second structural model proposed is the more likely one.

3.3 Bond-valence sum calculations

The bond-valence sums for $\text{RbKLi}_2[\text{Li}_3\text{SiO}_4]_4:\text{Eu}^{2+}$ were calculated using the bond-length/bond-strength concept (ΣV) [39, 40]. The charge distribution was derived using the CHARDI concept (CHARGE DIStribution in solids, ΣQ) [41, 42] (Table 8). Unfortunately, calculations according to the CHARDI concept are only possible for fully occupied atom sites. Therefore, two calculations for either of the fully occupied Li3 or Li4 sites were performed. The calculated formal ionic charges of all atoms are within the limits of the concepts, except the ΣV for the Li4 site. Li^+ on this site results in a charge of +0.41, which proves

Table 8: Charge distribution in $\text{RbKLi}_2[\text{Li}_3\text{SiO}_4]_4$, where only the Li3 site is occupied, calculated with the bond-length/bond-strength concept (ΣV) and the CHARDI concept (ΣQ).

	Rb1/K1	K2	Si1	Li1	Li2	Li3
ΣV	+0.97	+1.28	+3.36	+1.00	+0.99	+0.92
ΣQ	+1.10	+1.10	+4.04	+0.98	+0.99	+0.91
	O1	O2	O3			
ΣV	-2.03	-1.86	-2.13			
ΣQ	-2.13	-1.81	-2.24			

that an occupancy with lithium is unlikely. Calculating the bond-length/bond-strength for Eu^{2+} on this site on the other hand results in a charge of +2.61. Since Eu^{2+} is only incorporated in small amounts, just a slight deviation of the local structure surrounding the Eu^{2+} cation can be expected, which in turn would alter the calculated charge. Altogether, the bond valence sum calculations further support the plausibility of the proposed structural model. All values are listed in Tables 8 and 9.

3.4 Luminescence

Luminescence properties were measured on single crystals of the two different luminescent phases. For the excitation spectra and the determination of the thermal quenching behavior as well as the quantum efficiency, powder samples (Fig. 4) had to be used.

All samples showed an ultra-narrow-band emission upon excitation with near-UV to blue light. At a nominal activator concentration of 2 mol.%, blue emitting $\text{RbKLi}_2[\text{Li}_3\text{SiO}_4]_4:\text{Eu}^{2+}$ crystals have an emission maximum (λ_{max}) at 474 nm with a full width at half maximum (fwhm) of

Table 9: Charge distribution in $\text{RbKLi}_2[\text{Li}_3\text{SiO}_4]_4:\text{Eu}^{2+}$, where only the Li4 site is occupied, calculated with the bond-length/bond-strength concept (ΣV) and the CHARDI concept (ΣQ).

	Rb1/K1	K2	Si1	Li1	Li2	Li4/Eu ²⁺
ΣV	+0.97	+1.28	+3.36	+1.00	+0.99	+0.41/+2.61
ΣQ	+1.10	+1.10	+4.04	+0.98	+1.00	+0.91/-
	O1	O2	O3			
ΣV	-1.94	-1.86	-1.96			
ΣQ	-2.16	-1.81	-2.21			

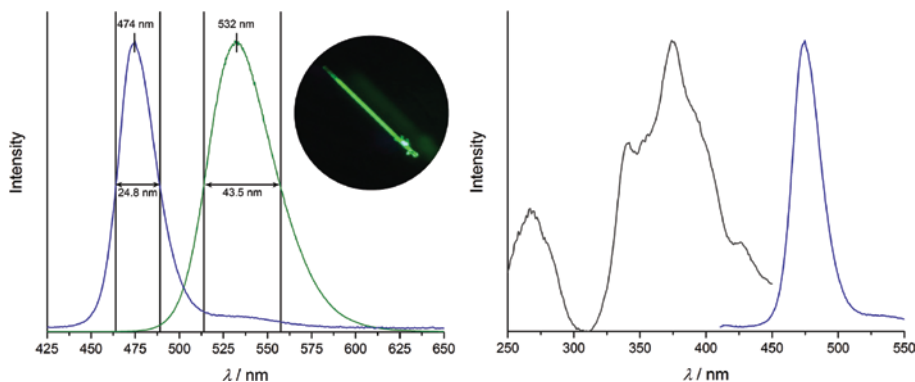


Fig. 5: Left: Luminescence spectra of the two single crystals of $\text{RbKLi}_2[\text{Li}_3\text{SiO}_4]_4:\text{Eu}^{2+}$ and a picture of the green luminescent single crystal under UV excitation (inlay). Right: Excitation spectrum of the blue emitting phase monitored at $\lambda_{\text{em}} = 474$ nm (gray) and emission spectrum with $\lambda_{\text{exc}} = 400$ nm (blue).

1107 cm^{-1} ($\approx 24.8\text{ nm}/0.137\text{ eV}$), while the green emitting ones have their maximum at 532 nm with a fwhm of 1523 cm^{-1} ($\approx 43.5\text{ nm}/0.193\text{ eV}$) (Fig. 5, left). Inside the CIE- xy color space, the blue phase is located at $x=0.120$ and $y=0.158$ and the green one at $x=0.259$ and $y=0.701$. It is important to stress the fact that according to the current state of knowledge, single crystals of $\text{RbKLi}_2[\text{Li}_3\text{SiO}_4]_4:\text{Eu}^{2+}$ show either a blue or a green luminescence as the main feature of the emission band. Of course, this cannot apply for powder samples since they always contain both phases.

An excitation spectrum was measured for a powder sample (Fig. 5, right), which primarily shows the ultra-narrow-band blue emission ($\lambda_{\text{max}} = 476\text{ nm}$). The emission at 476 nm shows its main excitability in the near UV spectral region with a $\lambda_{\text{exc}} = 374\text{ nm}$. Unfortunately, no bulk samples with the green emitting phase as the main

component could be obtained. Therefore, no excitation spectra could be measured.

Powder samples with the blue variant as the main phase were also used for measurements of the thermal quenching behavior (TQ) and the quantum efficiency (QE). Even this first unoptimized samples showed a QE of $\approx 50\%$ and a favorable TQ behavior. At $T = 225^\circ\text{C}$, the relative integrated intensity was still 76% of that at room temperature (Fig. 6).

When comparing the results presented in this paper with published data on other alkali lithosilicates crystallizing in the tetragonal space group $I4/m$, e.g. $\text{RbNa}_3[\text{Li}_3\text{SiO}_4]_4:\text{Eu}^{2+}$ ($\lambda_{\text{max}} = 471\text{ nm}/\text{fwhm} = 22.4\text{ nm}$), $\text{CsNa}_2\text{K}[\text{Li}_3\text{SiO}_4]_4:\text{Eu}^{2+}$, and $\text{RbNa}_2\text{K}[\text{Li}_3\text{SiO}_4]_4:\text{Eu}^{2+}$ (both $\lambda_{\text{max}} = 480/485\text{ nm}/\text{fwhm} = 25\text{ nm}$ and a second broader emission at $\lambda_{\text{max}} = 530\text{ nm}$), some similarities to $\text{RbKLi}_2[\text{Li}_3\text{SiO}_4]_4:\text{Eu}^{2+}$ are observed. All substances have similar luminescence properties, showing emission bands in the blue and/or green spectral region. However, in the case of the green variation of the $\text{RbKLi}_2[\text{Li}_3\text{SiO}_4]_4:\text{Eu}^{2+}$ phosphor presented here, it is the first time in the substance class of alkali lithosilicates crystallizing in the space group $I4/m$ that only one intense, ultra-narrow-band green emission is observed. Thanks to the unique structural properties of $\text{RbKLi}_2[\text{Li}_3\text{SiO}_4]_4:\text{Eu}^{2+}$, it was possible to link the observed green luminescence to the eight-fold cuboid surrounding of the activator ion Eu^{2+} inside the second type of channel based on single crystal X-ray diffraction data. This position would be similar to the Na site in $\text{RnLSO}:\text{Eu}^{2+}$ and $\text{C/RnKLSO}:\text{Eu}^{2+}$.

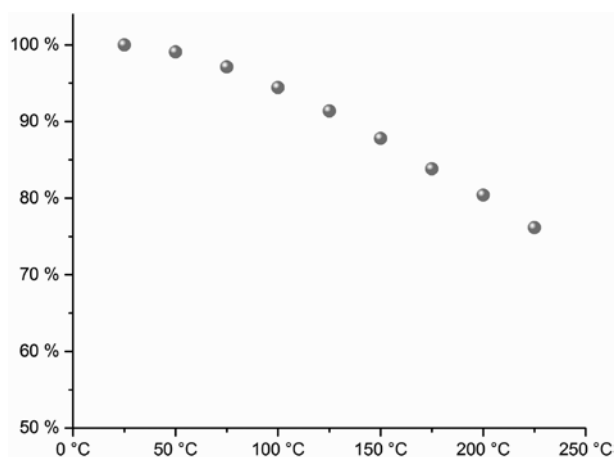


Fig. 6: The thermal quenching properties of $\text{RbKLi}_2[\text{Li}_3\text{SiO}_4]_4:\text{Eu}^{2+}$ in the temperature range of $25\text{--}225^\circ\text{C}$.

4 Conclusion

Here, we report on the new phosphor $\text{RbKLi}_2[\text{Li}_3\text{SiO}_4]_4:\text{Eu}^{2+}$ crystallizing in the tetragonal space group $I4/m$.

Two different types of this material could be synthesized, showing either a green or a blue emission. No exact classification exists whether an emission profile is described as broad-, narrow- or ultra narrow-band. As mentioned in the abstract we propose that the term ultra-narrow should be used exclusively for phosphors with a fwhm below 0.2 eV. The full width at half maximum of both phosphors presented here (green = 0.193 eV, blue = 0.137 eV) fulfill this criterion and can therefore be defined as ultra-narrow emitting.

The space group $I4/m$ is common in the material class of alkali lithosilicates, especially for those containing the heavy alkali cations rubidium or cesium. However, the structure presented here is the only known example where the second channel, containing the lighter alkali metal cations, incorporates exclusively lithium. Thanks to this unique configuration of this compound, it was possible to determine the exact positioning of the activator ion in the structure of the green luminescent modification via X-ray diffraction on single crystals. Therewith, it is possible to link the green Eu^{2+} emission in the alkali lithosilicates $\text{RKLSO}:\text{Eu}^{2+}$ and $\text{C/RNKLSO}:\text{Eu}^{2+}$ to the eight-fold cuboid coordinated atom site, which is unoccupied in the blue luminescent compound $\text{RKLSO}:\text{Eu}^{2+}$ or occupied by Na^+ in the case of $\text{C/RNKLSO}:\text{Eu}^{2+}$.

Furthermore, it is obvious that the blue luminescence cannot originate from Eu^{2+} located inside the “light alkali metal channel”, since no electron density could be found at the atom site in question. Therefore, the blue emission could be a result of a substitution of Rb^+ or K^+ by Eu^{2+} inside the other channel. Both atom sites show a highly symmetric, eight-fold, cuboid coordination. Therefore, a localization of the activator on both sites could be plausible and should be subject of further investigations.

Unfortunately, it is still unclear why and how the synthesis of $\text{RbKLi}_2[\text{Li}_3\text{SiO}_4]_4:\text{Eu}^{2+}$ yields these two different luminescent phases. This aspect needs to be in the focus of further investigations. However, the data presented here once more show the importance of single crystal analysis when dealing with hitherto unknown phosphors (especially with high Li content). Through an investigation on powder samples alone, the unique properties of these compounds probably would never have been discovered.

Acknowledgments: The authors would like to thank Christian Koch for the EDX measurements (OSRAM Opto Semiconductors).

References

- [1] D. Dutzler, M. Seibald, D. Baumann, H. Huppertz, *Angew. Chem. Int. Ed.* **2018**, *57*, 13676–13680.
- [2] K. Bernet, R. Hoppe, *Z. Anorg. Allg. Chem.* **1991**, *592*, 93–105.
- [3] H. Liao, M. Zhao, M. S. Molokeev, Q. Liu, Z. Xia, *Angew. Chem. Int. Ed.* **2018**, *57*, 11728–11731.
- [4] M. Zhao, H. X. Liao, L. X. Ning, Q. Y. Zhang, Q. L. Liu, Z. G. Xia, *Adv. Mater.* **2018**, *30*, 1802489.
- [5] M. Iwaki, S. Kumagai, S. Konishi, A. Koizumi, T. Hasegawa, K. Uematsu, A. Itadani, K. Toda, M. Sato, *J. Alloys Compd.* **2019**, *776*, 1016–1024.
- [6] M. Seibald, D. Baumann, T. Fiedler, S. Lange, WO 2017-EP70343, **2018**.
- [7] P. Strobel, C. Maak, V. Weiler, P. J. Schmidt, W. Schnick, *Angew. Chem. Int. Ed.* **2018**, *57*, 8739–8743.
- [8] P. Strobel, T. de Boer, V. Weiler, P. J. Schmidt, A. Moewes, W. Schnick, *Chem. Mater.* **2018**, *30*, 3122–3130.
- [9] P. Strobel, R. Niklaus, P. J. Schmidt, W. Schnick, *Chem. Eur. J.* **2018**, *24*, 12678–12685.
- [10] P. Pust, P. J. Schmidt, W. Schnick, *Nat. Mater.* **2015**, *14*, 454–458.
- [11] M.-H. Fang, J. L. Leañó, R.-S. Liu, *ACS Energy Lett.* **2018**, *3*, 2573–2586.
- [12] C. C. Lin, R.-S. Liu, *J. Phys. Chem. Lett.* **2011**, *2*, 1268–1277.
- [13] L. Chen, C.-I. Chu, R.-S. Liu, *Microelectron. Reliab.* **2012**, *52*, 900–904.
- [14] H. F. Sijbom, R. Verstraete, J. J. Joos, D. Poelman, P. F. Smet, *Opt. Mater. Express* **2017**, *7*, 3332–3365.
- [15] S. Li, R.-J. Xie, T. Takeda, N. Hirosaki, *ECS J. Solid State Sci. Technol.* **2018**, *7*, R3064–R3078.
- [16] T. Takeda, R.-J. Xie, T. Suehiro, N. Hirosaki, *Prog. Solid State Chem.* **2018**, *51*, 41–51.
- [17] S. Nakamura, *Rev. Mod. Phys.* **2015**, *87*, 1139–1151.
- [18] S. P. DenBaars, D. Feezell, K. Kelchner, S. Pimplutkar, C.-C. Pan, C.-C. Yen, S. Tanaka, Y. Zhao, N. Pfaff, R. Farrell, M. Iza, S. Keller, U. Mishra, J. S. Speck, S. Nakamura, *Acta Mater.* **2013**, *61*, 945–951.
- [19] R. J. Xie, N. Hirosaki, H. L. Li, Y. Q. Li, M. Mitomo, *J. Electrochem. Soc.* **2007**, *154*, J314–J319.
- [20] N. Hirosaki, R.-J. Xie, K. Kimoto, T. Sekiguchi, Y. Yamamoto, T. Suehiro, M. Mitomo, *Appl. Phys. Lett.* **2005**, *86*, 211905/211901–211905/211903.
- [21] J. Baur, P. Schlotter, J. Schneider, *Festkoerperprobleme* **1998**, *37*, 67–78.
- [22] T. Takahashi, S. Adachi, *J. Electrochem. Soc.* **2008**, *155*, E183–E188.
- [23] K. Uheda, N. Hirosaki, Y. Yamamoto, A. Naito, T. Nakajima, H. Yamamoto, *Electrochem. Solid-State Lett.* **2006**, *9*, H22.
- [24] K. Uheda, N. Hirosaki, H. Yamamoto, *Phys. Status Solidi A* **2006**, *203*, 2712–2717.
- [25] G. J. Hoerder, M. Seibald, D. Baumann, T. Schröder, S. Peschke, P. C. Schmid, T. Tyborski, P. Pust, I. Stoll, M. Bergler, *Nat. Commun.* **2019**, *10*, 1824.
- [26] P. Pust, V. Weiler, C. Hecht, A. Tucks, A. S. Wochnik, A. K. Henss, D. Wiechert, C. Scheu, P. J. Schmidt, W. Schnick, *Nat. Mater.* **2014**, *13*, 891–896.
- [27] Z. Xia, Q. Liu, *Prog. Mater. Sci.* **2016**, *84*, 59–117.

- [28] M. Seibald, T. Rosenthal, O. Oeckler, W. Schnick, *Crit. Rev. Solid State Mater. Sci.* **2014**, *39*, 215–229.
- [29] H. Moon, C. Lee, W. Lee, J. Kim, H. Chae, *Adv. Mater.* **2019**, Ahead of Print (DOI: 10.1002/adma.201804294).
- [30] SAINT (version 8.34a), Bruker AXS Inc., Madison, Wisconsin (USA) **2014**.
- [31] G. M. Sheldrick, SADABS (version 2014/5), Bruker AXS Inc., Madison, Wisconsin (USA) **2001**.
- [32] WIN XPOW (version 2.23), STOE & Cie GmbH, Darmstadt (Germany) **2005**.
- [33] G. M. Sheldrick, *Acta Crystallogr.* **2008**, *A64*, 112–122.
- [34] TOPAS (version 4.2), Bruker AXS Inc., Madison, Wisconsin (USA) **2009**.
- [35] J. Hoffmann, R. Brandes, R. Hoppe, *Z. Anorg. Allg. Chem.* **1994**, *620*, 1495–1508.
- [36] M. Zhao, Y. Zhou, M. S. Molokeev, Q. Zhang, Q. Liu, Z. Xia, *Adv. Opt. Mater.* **2019**, *7*, 1801631.
- [37] F. Liebau, *Structural Chemistry of Silicates*, Springer, Berlin, Heidelberg, **1985**.
- [38] R. Shannon, *Acta Crystallogr.* **1976**, *A32*, 751–767.
- [39] I. D. Brown, D. Altermatt, *Acta Crystallogr.* **1985**, *B41*, 244–247.
- [40] N. Brese, M. O’Keeffe, *Acta Crystallogr.* **1991**, *B47*, 192–197.
- [41] R. Hoppe, *Z. Kristallogr.* **1979**, *150*, 23–52.
- [42] R. Hoppe, S. Voigt, H. Glaum, J. Kissel, H. P. Müller, K. Bernet, *J. Less-Common Met.* **1989**, *156*, 105–122.